Influence of forced near-inertial motion on the kinetic energy of a nearly-geostrophic flow

Stephanne Taylor and David Straub

McGill University
stephanne.taylor@mail.mcgill.ca

Abstract

The effect of forced near-inertial motion on the kinetic energy budget of a turbulent, geostrophic background flow is examined using a primitive equation ocean circulation model. Balanced and unbalanced parts of the flow are taken to be equivalent to low- and high-passed filtered versions of the model fields, and the Reynolds stresses associated with the high-passed, predominantly near-inertial part of the flow are found to extract low frequency kinetic energy. Transfer spectra show that this transfer occurs at wavenumbers close to the deformation wavenumber, ie, at mesoscale wavenumbers. Whether or not this "advective sink" results in a reduction of low frequency kinetic energy is found to be sensitive to model resolution and to a pressure work term which is peaked a higher horizontal wavenumber and transfers energy between the balanced potential and kinetic energy pools.

1 Introduction

Whether balanced-to-unbalanced energy transfers and a subsequent forward cascade of unbalanced motion acts as a significant sink for the ocean's mechanical energy budget has been a source of ongoing speculation and interest. In the absence of high frequency forcing or rough topography, a variety of studies on initially-balanced flows indicate that such transfers are weak (e.g., Molemaker et al. (2010); Ngan et al. (2008); Zeitlin (2008); Vanneste (2008, 2013)). Observations and realistic modelling studies, by contrast, routinely show balanced and near-inertial motion to co-exist in the oceans, and realistic forcing fields directly project onto both (Ferrari and Wunsch, 2009). This has led to consideration of balanced-to-unbalanced energy transfers in settings where unbalanced motions were either initially present at significant levels or was externally forced (e.g., Bühler and McIntyre (2005); Gertz and Straub (2009); Xie and Vanneste (2015); Whitt and Thomas (2015); Taylor and Straub (2016); Grisouard and Thomas (2016); Barkan et al. (2016)).

Our focus is on balanced-to-unbalanced kinetic energy (KE) transfers in a moderate Rossby number, primitive equation channel. Balance and imbalance are taken to be the low- and high-pass filtered portions of the motion. A key element of this study is that the high frequency modes are externally forced: without this forcing—and for the moderate Rossby numbers typical of most oceanic settings—frequency energy spectra show little energy in the near-to-super-inertial bands. With external forcing, near-inertial motion is excited and exerts Reynolds stresses on the balanced flow. This typically results in a loss of balanced kinetic energy which we will refer to as the "advective sink". We define the advective sink as $\chi = \mathbf{u}^{<} \cdot [\nabla \cdot (\mathbf{v}^{>}\mathbf{u}^{>})]^{<}$, with $\mathbf{v}^{>}$ including the vertical velocity component. This form of the transfer term respects the model numerics, which represents the advective terms in flux form.

In this context, the model of Xie and Vanneste (2015) is of particular interest. It considers a superposition of balanced flow and unbalanced modes, which are formally restricted to be near-inertial but can have arbitrary horizontal length scale. As with the advective sink mechanism mentioned above, balanced-to-unbalanced transfer occurs only if the unbalanced modes are externally forced or are present in initial conditions. By contrast, however, the advective sink mechanism appears to be explicitly filtered in this framework. It thus appears that the two mechanisms are distinct, with the advective sink involving KE transfers and the Xie and Vanneste interaction involving PE transfers. An alternative interpretation would be that the advective sink transfers could be coupled to KE-to-PE transfers within the high frequency energy pool. This latter interpretation is consistent with the results of Claret et al. (2016), which considers the interaction of wind generated near-inertial waves with a baroclinic front in a 2-dimensional Boussinesq context.

In previous work (Taylor and Straub, 2016), we considered a zonally periodic primitive equation channel forced by a combination of steady and high frequency winds. The high-frequency forcing excites near-inertial motion and our focus was on how this influences the low-frequency, nearly geostrophic part of the flow. A key finding was that at moderate geostrophic Rossby number, addition of high frequency forcing led to a decrease in low-frequency kinetic energy associated with the advective sink. Transfer spectra showed these transfers to occur predominately in the mesoscale, i.e., at horizontal scales comparable to the deformation radius. They were thus well resolved by our eddy-permitting resolution.

This short contribution considers similar simulations, but with better horizontal and vertical resolution. We find that improved resolution leads to a significant increase in the balanced-to-unbalanced kinetic energy transfers. Because these transfers remain predominately in the mesoscale and tend to be dominated by terms involving vertical derivatives, we infer that this increase is related to improved vertical resolution. For a given (balanced) base state, stronger high frequency forcing leads to stronger transfers. Unlike our previous results, however, low frequency KE is not seen to decrease in association with this balanced kinetic energy sink: instead, it increases. This behavior was also noted in Taylor and Straub (2016), but only in the low Rossby number base state simulations. We attribute the increase in KE to the pressure work term, which is associated with PE-to-KE transfers within the pool of balanced energy. The pressure work transfer spectra are somewhat noisy transfers and peaked at higher horizontal wavenumbers than the advective sink. As such, they are sensitive to horizontal resolution, consistent with the result mentioned above. This increased balanced PE-to-KE transfer is likely related to another influence of wind-driven near-inertial motion: it introduces vertical shear which can lead to a deepening of the surface mixed layer. This changes the stratification, thus affecting baroclinic instability and the related energy transfers.

2 Setup

We consider a wind-driven channel flow in a spherical coordinate primitive equation model (POP). The channel is 4000 m deep, 60° long and extends from 43° to 67° south, and the domain spans 780 × 528 × 30 grid points. This corresponds to a resolution of about 5 km in the meridional direction and between 3.3 and 6.2 km in the zonal direction. The deformation radius, L_D, is about 20-22 km, so that L_D^{-1} corresponds to a nondimensional wavenumber in the low 30s. Vertical grid spacing ranges from 10 to 300 m thick. A

meridional Gaussian ridge provides form drag, which is necessary to balance the zonal momentum budget. We use a linear, single component equation of state and apply biharmonic viscosity in the horizontal and use a KPP scheme in the vertical. A quadratic bottom drag dissipates the bulk of the kinetic energy.

Wind forcing includes both steady and near-inertial components. The steady wind has a sinusoidal meridional profile, and is strongest in the middle of the channel:

$$\tau_{\text{steady}} \equiv \tau_0 \Big(1 + \cos(2\pi(\theta - \theta_0)/\Delta\theta) \Big) \tag{1}$$

where θ_0 is the latitude of the middle of the channel, and $\Delta\theta$ is the difference in latitude between the edges of the fluid. We use four values of τ_0: $0.30, 0.15, 0.03$, and 0.015 N m^{-2}, and refer to them as strong, medium, weak, and very weak respectively. The medium value of $\tau_0 = 0.15$ N m^{-2} roughly corresponds to the average wind stress over the Southern Ocean in winter (Li et al., 2013).

The time-varying wind is explicitly truncated at frequencies of $f/2$ and $2f$ so that it does not project on to the low frequency motion. We define

$$\tau^x_{\text{NI}}(t) \equiv \xi\tau_0 \sum_{n=1}^{N} N^{-0.5} \exp\Big(- \frac{(\omega_n - f_0)^2}{2\sigma^2} \Big) \sin(\omega_n t + \phi_n) \tag{2}$$

where f_0 is the Coriolis frequency at the middle of the channel, $\sigma = f_0/6$, and ω_n ranges from $f_0/2$ to $2f_0$ and is linearly sampled with $N = 10,000$. Scaling τ^x_{NI} with the strength of the steady forcing allows straightforward comparison of results between the different base states; we use three values of $\xi = \{0.2, 0.35, 0.5\}$. The near-inertial wind forcing has no spatial structure.

The model is spun up with the steady wind forcing for 20, 40, 85, and 125 years for $\tau_0 = \{0.30, 0.15, 0.03, 0.015\}$ N m^{-2} respectively. Following spin-up, we continue the integration using both the steady and near-inertial winds: two years to allow for adjustment to the added forcing and further 27 months used in our analysis. We use Fourier methods to separate the low- and high-passed fields, e.g., respectively $\mathbf{u}^<$ and $\mathbf{u}^>$ for horizontal velocity; other quantities are treated similarly. Figure 1 shows typical snapshots of the flow in the middle of the 27 month data collection window for the medium base state ($\tau_0 = 0.15$ N m^{-2}.) The left panel shows the full flow for the control run, with partial topographic contours overlaid in red to indicate the position of the meridional ridge. The right panel shows surface values of $\mathbf{u}^>$ for $\xi = 0.35$. Note that the amplitude of near-inertial motion is relatively consistent over the horizontal extent of the domain.

3 Results

Four main terms dominate the balanced kinetic energy budget (Figure 2): (i) the steady wind input, (ii) bottom drag, (iii) the advective sink, and (iv) the low-frequency pressure work term. Note that there is also a non-geostrophic, Ekman-like component to the low frequency flow; this is dissipated by the vertical viscosity and will not be considered further. Although generally we use a frequency spectral filter to separate balanced and unbalanced motion, for some terms (namely, the wind power input, the dissipation due to

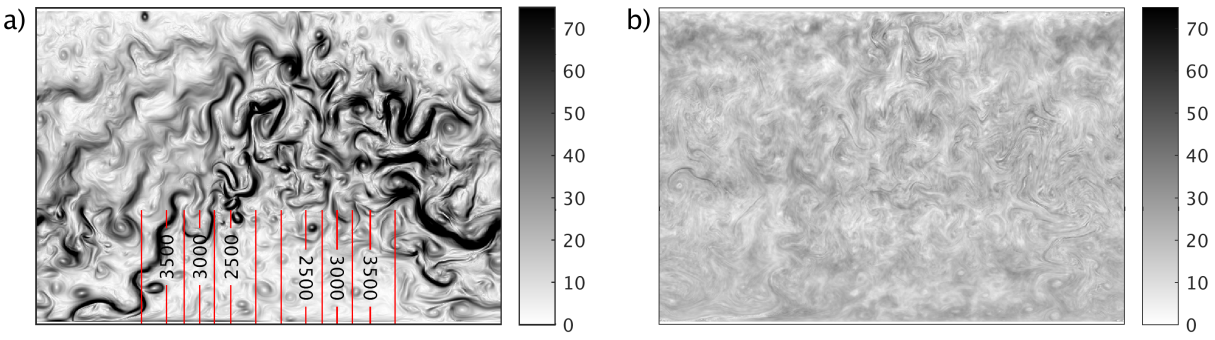

Figure 1: Typical snapshots of the surface speed (units are cm s^{-1}). Panel (a) shows the control run, and panel (b) shows high frequency flow for $\tau_0 = 0.15$N m^{-2}, $\xi = 0.35$. Panel (a) also shows partial topographic contours; contours extend the breadth of the channel but are shown only at the bottom edge to avoid obscuring the energetic flow. The channel spans 60° longitude and 24° latitude.

bottom drag, and dissipation due to viscosity), we found it convenient to use geostrophy as a proxy for balance.[1]

From Figure 2(a), it is evident that the steady wind input does not vary significantly with ξ and that bottom drag is the dominant route to dissipation. Horizontal viscosity is negligible and vertical viscosity acts primarily on the ageostrophic motion near the surface. The sum of the geostrophic wind input and bottom drag is shown in dotted lines in Figure 2(a). This residual is balanced primarily by a combination of the advective sink and the pressure work (panels (b) and (c) respectively). These two terms are comparable in magnitude, but have trends of opposite signs. The advective sink can balance up to 20% of the total work done by the steady wind and over 30% of the wind work done on the geostrophic flow. There is a clear dependence on both the base state and ξ: more energetic base states and stronger higher frequency forcing both lead to larger advective sinks.

The reduction of balanced KE due to the advective sink is more than offset by the changes in pressure work. For our control ($\xi = 0$) simulations, pressure work converts KE to PE. Addition of even a small amount of near-inertial forcing reverses this, and the resulting balanced PE-to-KE transfer offsets the advective sink. Note also that, while the magnitude of the advective sink is dependent on the base state, this dependence is much reduced for the pressure work. We speculate that the change of sign in the pressure work term is related to enhanced baroclinic instability resulting from a deepening of the surface mixed layer. This deepening results from enhanced vertical mixing due to vertical shear introduced by the near-inertial modes.

We focus, then, on the advective sink, χ. Its magnitude depends on τ_0, although its horizontal and vertical spatial structure essentially do not. Vertical profiles of the horizontally averaged advective sink are shown in Figure 3(a). It seems that χ serves largely to transfer balanced energy downward—the sign change is near the base of the surface mixed layer. However, more energy is extracted from the mixed layer than is deposited below, so that a net sink results. The horizontal structure of the advective sink can be analyzed by considering transfer spectra, shown in Figure 3(b). Because we use spherical coordinates, an adjustment to the 2D latitude-longitude FFT is applied so that the bins

[1]It is straightforward to calculate the wind input using the spectral filter; however, this includes forcing of the Ekman-like flow in the surface layers which, as mentioned, is not our focus here.

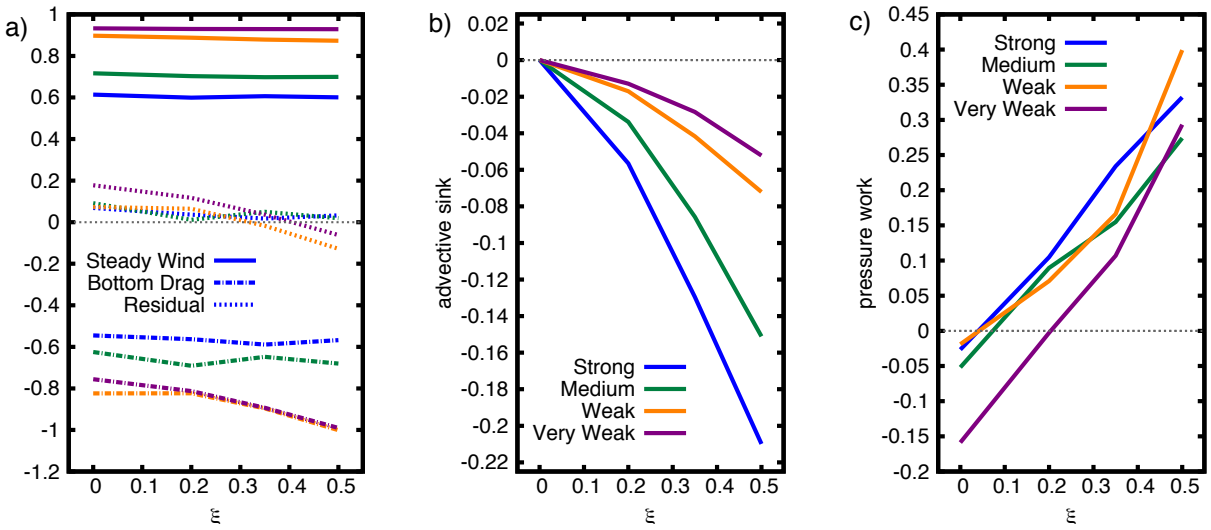

Figure 2: The kinetic energy budget for the balanced flow (viscosity is omitted). Wind input and bottom drag are calculated using geostrophic flow, while the advective sink and pressure work are calculated with low-passed flow. Panel (a) shows steady wind input (solid lines), dissipation by bottom drag (dot-dash lines), and their sum (dashed lines). Their sum is primarily balanced by the advective sink (panel (b)) and pressure work (panel (c)). Note that while the steady wind input barely changes with increasing ξ and the bottom drag shows a weak response, the advective sink and pressure work strongly depend on the level of near-inertial forcing. Colour scheme is consistent across all panels.

correspond as closely as possible to physical length scales. This is described in Appendix B of Taylor and Straub (2016).[2]

Transfer spectra for the advective sink in the surface layer with $\xi = 0.35$ are shown in solid lines in Figure 3(b). In all base states, the advective sink removes low frequency energy from the mesoscale: the upper ocean transfer spectra consistently peak at around $\kappa = 20$, which corresponds to a length scale of ~ 35 km. Below the mixed layer where $\chi > 0$, the (positive) spectra peak at a lower wavenumber. In the deep ocean, the spectra are noisy, flat, and slightly positive. Also shown in dashed lines are surface layer transfer spectra for a high frequency kinetic counterpart to χ: $\chi_{\mathrm{HF}} = \mathbf{u}^{>} \cdot (\nabla \cdot (\mathbf{v}^{>}\mathbf{u}^{<}))$.[3] In the high frequency energy equation, both a forward cascade and a net source are evident. Integrated vertically and over horizontal wavenumber, the advective sink χ is balanced by χ_{HF}; additionally, the forward cascade is reduced in vertically integrated profiles of χ_{HF}. The peak wavenumber in χ_{HF} transfer spectrum is somewhat higher than that for χ, but nonetheless remains close to $k_h = 1/L_D$.

4 Discussion

We consider the influence of wind-driven near-inertial motion on the low-frequency kinetic energy budget of a nearly-geostrophic, primitive equation channel flow. The Rossby radius is resolved with about four grid points. Following oceanographic jargon, this hori-

[2]Briefly, this scheme splits the 2D FFT calculation into three parts: a 1D zonal FFT at each latitude, a reorganization of the data so that the zonal bins correspond to consistent physical wavelengths at all latitudes, and then a 1D meridional FFT. As our grid is as isotropic as possible, this adjustment results in only a small correction to our spectra.

[3]χ_{HF} differs from χ by the divergence of a flux, which is visible in Figure 3(b).

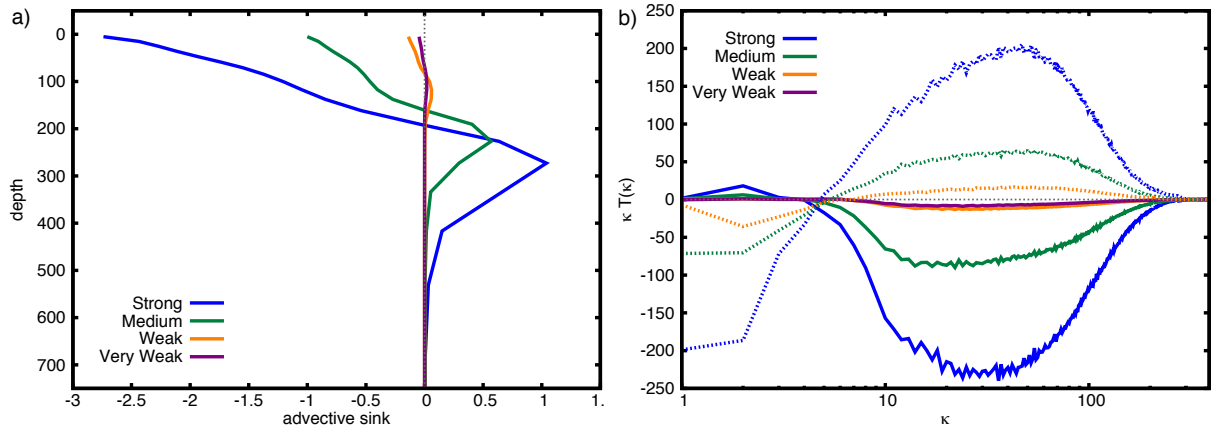

Figure 3: Spatial structure of the advective sink for various base states and $\xi = 0.35$. Panel (a) shows vertical profiles in the upper ocean; all local values are small in the abyss. Panel (b) shows horizontal transfer spectra at the surface for both the low frequency advective sink χ (solid) and the high frequency corollary χ_{HF} (dashed).

zontal resolution is better than "eddy permitting" but does not adequately represent the submesoscale. We find that Reynolds stresses exerted by the near-inertial flow serve to extract low frequency kinetic energy. Transfer spectra show this extraction to be well resolved at this, and even lower, resolution. The near-inertial motion also serves to excite vertical shear in the horizontal velocity near the base of the surface mixed layer. This deepens the mixed layer, affecting upper ocean stratification. Likely related to this, the pressure work term responsible for exchanges between low frequency potential and kinetic energy is also sensitive to the near-inertial forcing. These transfers are noisy and peaked at relatively high wavenumber. Finally, we note that the advective sink considered here is only part of the story: how it relates to other mechanisms, such as the balanced-to-unbalanced transfer mechanism proposed by Xie and Vanneste (2015), as well as how forced near-inertial flow affects the potential energy budget are left to future work.

References

Barkan, R., Winters, K., and McWilliams, J. C. (2016). Stimulated imbalance and the enhancement of eddy kinetic energy dissipation by internal waves. submitted to Journal of Physical Oceanography.

Bühler, O. and McIntyre, M. E. (2005). Wave capture and wave-vortex duality. *Journal of Fluid Mechanics*, 534:67–95.

Claret, M., Tandon, A., Polzin, K., and Mahadevan, A. (2016). Escape of near-inertial waves trapped in strong fronts through wave-triad resonant interactions. submitted to Journal of Physical Oceanography.

Ferrari, R. and Wunsch, C. (2009). Ocean circulation kinetic energy: Reservoirs, sources, and sinks. *Annual Review of Fluid Mechanics*, 41:253–282.

Gertz, A. and Straub, D. N. (2009). Near-inertial oscillations and the damping of mid-latitude gyres: A modeling study. *Journal of Physical Oceanography*, 39(9):2338–2350.

Grisouard, N. and Thomas, L. N. (2016). Energy exchanges between density fronts and

near-inertial waves reflecting off the ocean surface. *Journal of Physical Oceanography*, 46:501–516.

Li, M., Liu, J., Wang, Z., Wang, H., Zhang, Z., Zhang, L., and Yang, Q. (2013). Assessment of sea surface wind from nwp reanalyses and satellites in the southern ocean. *Journal of Atmospheric and Oceanic Technology*, 30:1842–1853.

Molemaker, M. J., McWilliams, J. C., and Capet, X. (2010). Balanced and unbalanced routes to dissipation in an equilibrated eady flow. *Journal of Fluid Mechanics*, 654:35–63.

Ngan, K., Bartello, P., and Straub, D. (2008). Dissipation of synoptic-scale flow by small-scale turbulence. *Journal of the Atmospheric Sciences*, 65(3):766–791.

Taylor, S. and Straub, D. (2016). Forced near-inertial motion and dissipation of low-frequency kinetic energy in a wind-driven channel flow. *Journal of Physical Oceanography*, 46:79–93.

Vanneste, J. (2008). Exponential smallness of inertia-gravity wave generation at small rossby numer. *Journal of the Atmospheric Sciences*, 65:1622–1637.

Vanneste, J. (2013). Balance and spontaneous wave generation in geophysical flows. *Annual Review of Fluid Mechanics*, 45:147–172.

Whitt, D. B. and Thomas, L. N. (2015). Resonant generation and energetics of wind-forced near-inertial motions in a geostrophic flow. *Journal of Physical Oceanography*, 45:181–208.

Xie, J.-H. and Vanneste, J. (2015). A generalised-lagrangian-mean model of the interactions between near-inertial waves and mean flow. *Journal of Fluid Mechanics*, 774:143–169.

Zeitlin, V. (2008). Decoupling of balanced and unbalanced motions and inertia-gravity wave emission: Small versus large rossby numbers. *Journal of the Atmospheric Sciences*, 65:3528–3542.